Mining, Metallurgy & Exploration
https://doi.org/10.1007/s42461-025-01432-9

# Geological and Geophysical Survey of Mineral Resources with an Emphasis on Gold and Associated Minerals in Atshan area,South Eastern Desert, Egypt

**Mahdy Kh Abd-Elsadek[1] · S. A. S. Araffa[2] · Mohamed Aldeep[2] · Hazem Badreldin[2,4] · Adel A. A. Othman[3] · Waheed H. Mohamed[3] · Khaled Zaghlol[1]**

Received: 20 January 2025 / Accepted: 23 November 2025


**Abstract**
This study focuses on geological mapping and geophysical surveys to explore gold and associated mineral resources in the Atshan area, situated southwest of Marsa Alam city in the Red Sea region, Egypt. Gold occurrences and disseminated sulfides are localized within a shear zone that spans the area's western, central, and south-eastern parts, predominantly composed of metavolcanic rocks such as metabasalts and metaandesites. Chemical analyses of rock samples collected from various locations identified multiple gold anomalies, with concentrations ranging from 0.6 to 2.3 ppm. Magnetic, electrical resistivity (Rho), and induced polarization (IP) surveys were conducted to investigate the shear zone's structural trends, mineralization patterns, and subsurface extensions. Magnetic data were processed and interpreted using advanced techniques, including Total Magnetic Intensity (TMI), First Vertical Derivative (FVD), Horizontal Derivative (HDR), Radially Averaged Power Spectrum, and Source Parameter Imaging (SPI) maps, analyzed via Geosoft Oasis Montaj. Results revealed significant magnetic anomalies in the southwestern, south-eastern, and central parts, with high-amplitude values exceeding 41,440 nanoTesla (nT.) and depths ranging from 5 to 40 m. The resistivity and induced polarization surveys identified zones of low resistivity and high chargeability, corresponding to altered and sheared intermediate metavolcanic rocks. These zones are associated with sulfide mineralization containing encapsulated gold and other minerals, likely controlled by structural features. The primary structural trends determined from both surface geological observations and geophysical data are oriented in NE-SW, E-W, and NW-SE directions, reflecting the influence of the regional tectonic framework on mineralization processes.

**Keywords** Gold mineralization · Atshan area · Ground magnetic · Resistivity · And chargeability

## 1 Introduction

The Arabian-Nubian Shield (ANS), a well-endowed Neoproterozoic tectonic province, hosts numerous gold and base metal deposits, many of which have been mined since Pharaonic times, underscoring the region's enduring economic significance. The South Eastern Desert (SED) of Egypt, forming a critical part of the ANS, is characterized by a complex geological framework comprising ophiolitic assemblages, island arc volcanics, and granitoid intrusions. This intricate assembly creates a highly prospective terrane for various mineralization styles, with gold occurrences being predominantly structurally controlled. These are typically associated with shear zones, quartz veins, and hydrothermally altered metavolcanic and granitoid rocks.

✉ S. A. S. Araffa
sultan_awad@yahoo.com

1 Egyptian Mineral Resources Authority (EMRA), Cairo, Egypt

2 National Research Institute of Astronomy and Geophysics (NRIAG), Helwan, Cairo, Egypt

3 Geology Department, Faculty of Science, Al-Azhar University,, Cairo, Egypt

4 National Institute of Oceanography and Applied Geophysics, OGS, Via Treviso 55, Udine 33100, Italy

Published online: 22 December 2025

Significant research has been conducted within the SED, leading to the discovery and characterization of major deposits such as Sukari, Hamash, and Abu Marawat. These studies have employed a diverse range of techniques, including geophysical surveys [1], remote sensing [2], and structural analysis, providing invaluable insights into the regional metallogeny. Furthermore, comparative studies from analogous terranes globally, such as in India [3] and Brazil, consistently demonstrate the effectiveness of integrated geological and geophysical approaches for mineral exploration in structurally complex environments.

The Atshan study area, situated southwest of Marsa Alam city (between latitudes 24° 13′ 45″ and 24° 17′ 00″ N and longitudes 35° 11′ 00″ and 35° 14′ 15″ E, is located within this prospective Hamata district of the SED Fig. 1. The area exhibits promising gold anomalies. It is situated within a significant shear zone hosted in metavolcanic rocks. Mineralization in this area is structurally controlled, influenced by the interplay of regional metamorphism, granitic intrusions, and metavolcanic host rocks [4], with sulfides often occurring as disseminations within talc-tremolite rocks [5–12].

Despite the extensive regional research, detailed studies integrating high-resolution ground geophysical data with surface geology to understand localized mineralization controls in specific areas like Atshan remain limited. Many existing explorations suffer from insufficient geophysical resolution or a lack of updated structural reanalysis, constraining the effective targeting of subsurface ore bodies. Consequently, the precise spatial relationship between geophysical signatures (magnetic, resistivity, and induced polarization), the dominant structural trends, and the known gold mineralization in the Atshan area is not yet fully quantified or exploited for exploration targeting.

To address this knowledge gap, this study employs a dedicated integrated approach combining geological mapping (based on published maps and field verification), geochemical analysis, and detailed ground geophysical surveys, including magnetic, resistivity, and induced polarization methods in the Atshan area. The primary objectives are to delineate the subsurface architecture and identify key structural lineaments controlling fluid flow and mineralization. Characterize geophysical anomalies (magnetic highs, low resistivity, and high chargeability) indicative of

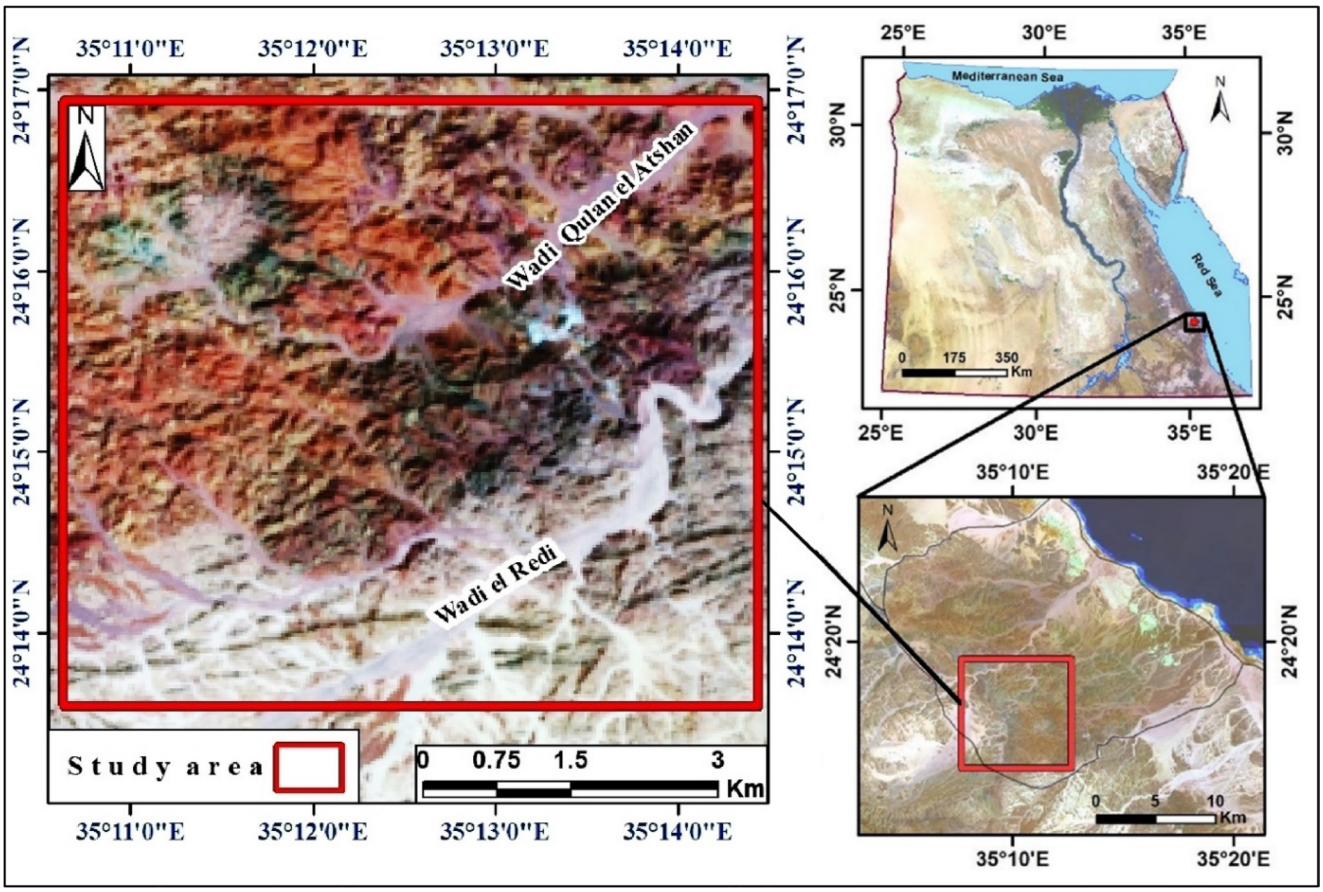


**Fig. 1** Location map of the investigated area

alteration and sulfide mineralization. Synthesize geological, geochemical, and geophysical datasets to define high-priority targets for gold and associated minerals. This work aims to provide a refined, data-driven exploration model for the Atshan area that can also be applied to similar geological settings within the ANS, thereby enhancing the efficacy of future mineral exploration campaigns.

## 2 Geologic Setting

The Hamata sediments, situated within the Eastern Desert, predominantly comprise Neoproterozoic basement rocks. These include gneisses and an ophiolitic mélange characterized by serpentinites, metagabbro, and metabasalts, later intruded by volcanic rocks and late-orogenic granitoids [13–16]. The metavolcanic rocks in the region are categorized into intermediate and basic types, such as low-grade metaandesites, metabasalts, and meta-porphyries, as well as acidic types, including metarhyolites and metarhyodacites [17–21]. Based on field investigations and insights from prior studies, a specific area within Hamata was selected for detailed analysis.

The exposed basement rocks in the research area consist mainly of island arc metavolcanics and granodiorites. These units are intersected by dikes, narrow carbonate veins, and quartz veins (Fig. 2). The rock formations are systematically described in order from oldest to youngest.

The geological map (Fig. 2) reveals that island arc rocks dominate the basement geology, making up approximately 80% of the area. These rocks are dark green in color and primarily consist of basic to intermediate metavolcanics, including metabasalt and metaandesite. The metavolcanic units are heavily sheared and foliated along shear zones, forming moderate to high hills (Fig. 3a and b).

Island arc metavolcanics are predominantly found in the northern and central parts of the area (Fig. 2). They are intersected by numerous quartz veins and crosscut by various joint sets (Fig. 3c). In areas associated with gold mineralization, quartz veins ranging from 50 cm to 1 m in width are observed, exhibiting various orientations (Fig. 3d). These quartz veins often form stockworks that contain visible sulfide crystals and are associated with alteration zones of varying sizes, typically between 1 and 5 m (Fig. 3e). The arc granitoids, predominantly granodiorites, are mainly located in the southern part of the study area (Fig. 2). These rocks form low-lying masses with a grayish-white coloration and granodioritic composition. They are extensively jointed (Fig. 4a), display spheroidal weathering, and are intersected by numerous quartz veins measuring 30 to 50 cm in width, striking NE-SW and dipping SE (Fig. 4b). Within the framework of plate tectonic theory, these granitoids are comparable to

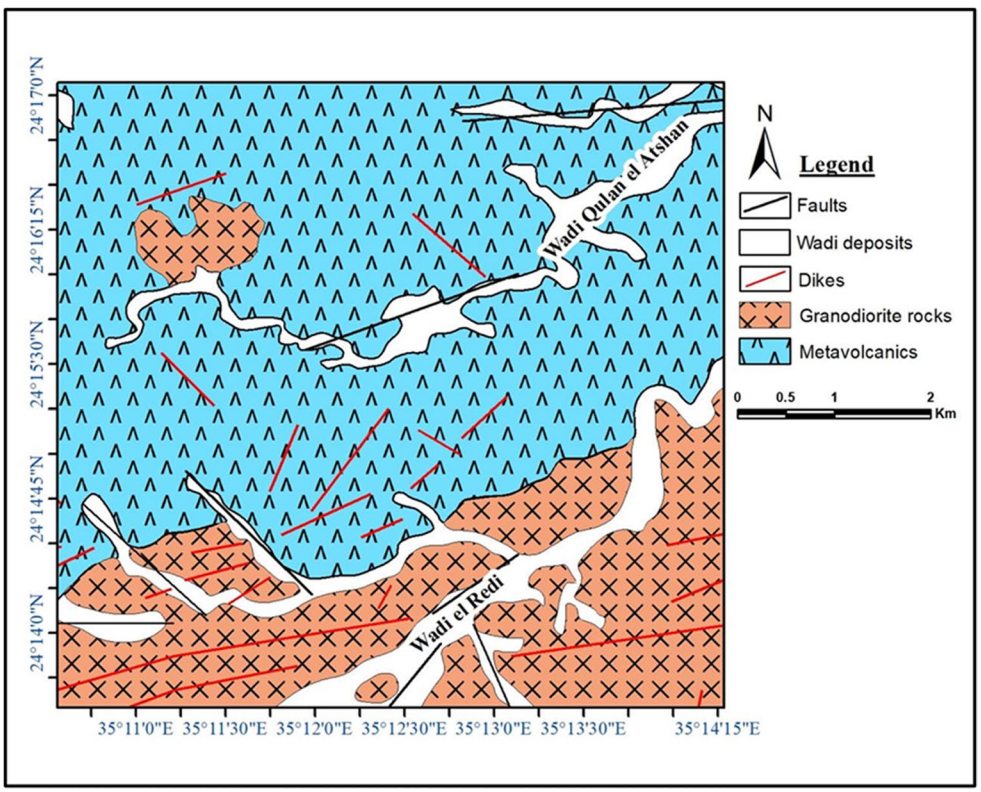


**Fig. 2** Simplified Geological map showing the study area. Modified after [22–24]

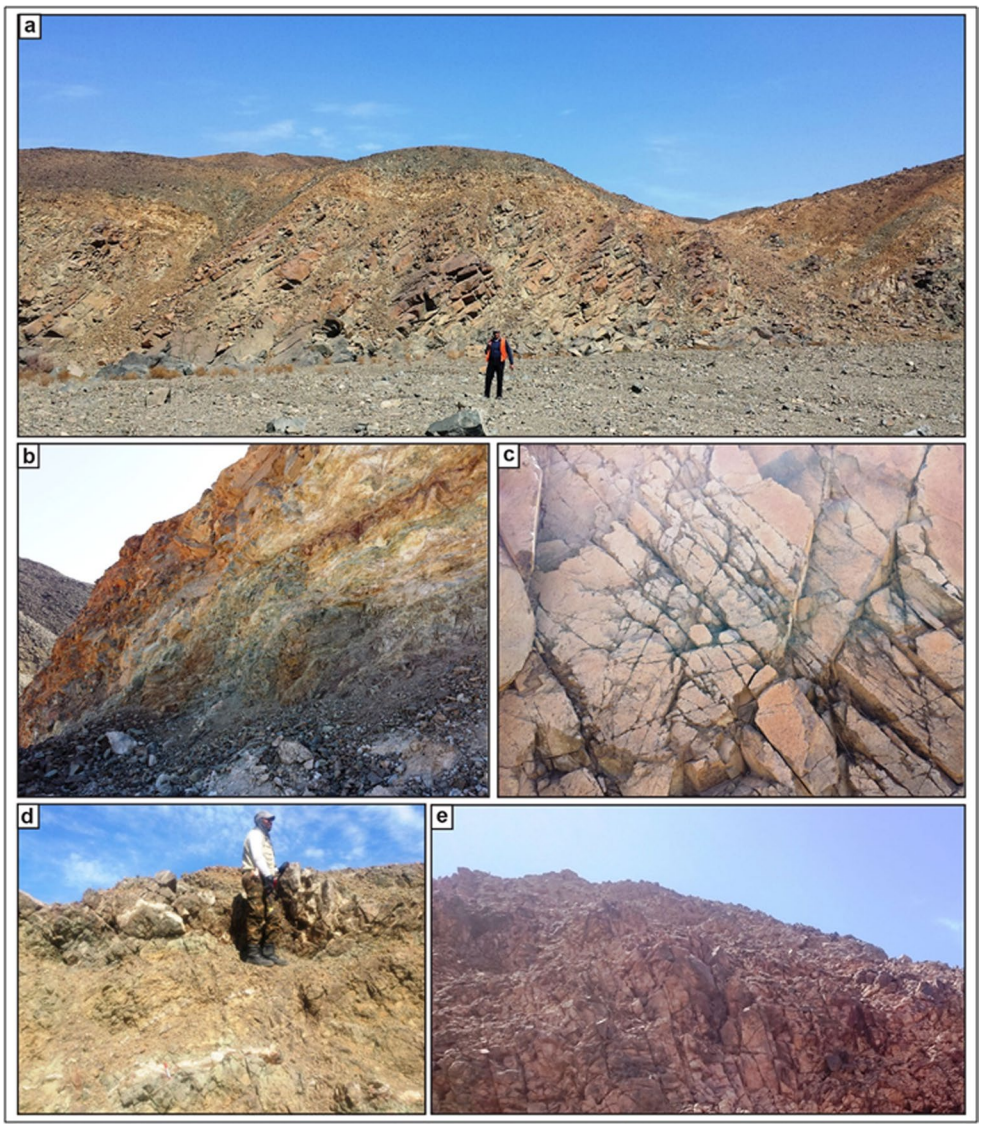


**Fig. 3** Field photographs, (**a**) Panoramic view of the island arc metavolcanics in Wadi Qulan el Atshan (Looking SW), (**b**) Highly sheared metavolcanics in Wadi Qulan el Atshan (Looking SW), (**c**) Close-up view of the island arc metavolcanics dissected by many joint sets, (**d**) A quartz vein cutting across the island arc metavolcanics in Wadi Dendekan (Looking NW), (**e**) Alteration zone surrounding quartz vein cutting across metavolcanic rocks in Wadi Dendekan (Looking NW)

subduction-related arc granitoids, often referred to as G1 granitoids [25] or I-type granites [26].

## 2.1 Dikes

Both metavolcanics and granodiorites in the area are intersected by basic and acidic dikes, indicating that these dikes represent the youngest intrusive events.

- **Basic dikes** are dark-colored, predominantly doleritic and basaltic in composition, with thickness ranging between 1 m and 2 m. These dikes are heavily jointed, and many of the joints are secondarily filled with brownish-red iron oxides (Fig. 4c).
- **Acidic dikes** are fine-grained and pinkish in color, reflecting their high alkali-feldspar content. They can reach up to 2 m in thickness (Fig. 4d).

The age relationship between the basic and acidic dikes remains uncertain, as no contact relationships between them were observed in the area.

## 2.2 Occurrence and Geochemistry of the Ore Deposit

The gold occurrence in the Atshan area is associated with the quartz veins that accompany many deposits, including the talc deposits, where gold is found within quartz veins that dissect the alteration zones hosted in metavolcanic rocks. These zones are intersected by granodiorite intrusions and basic to acidic dikes, with recent deposits covering gentle mountain slopes and wadis. In this region, gold-bearing quartz veins are associated with well-developed alteration zones, ranging from 2 to 6 m in thickness (see Fig. 3e).

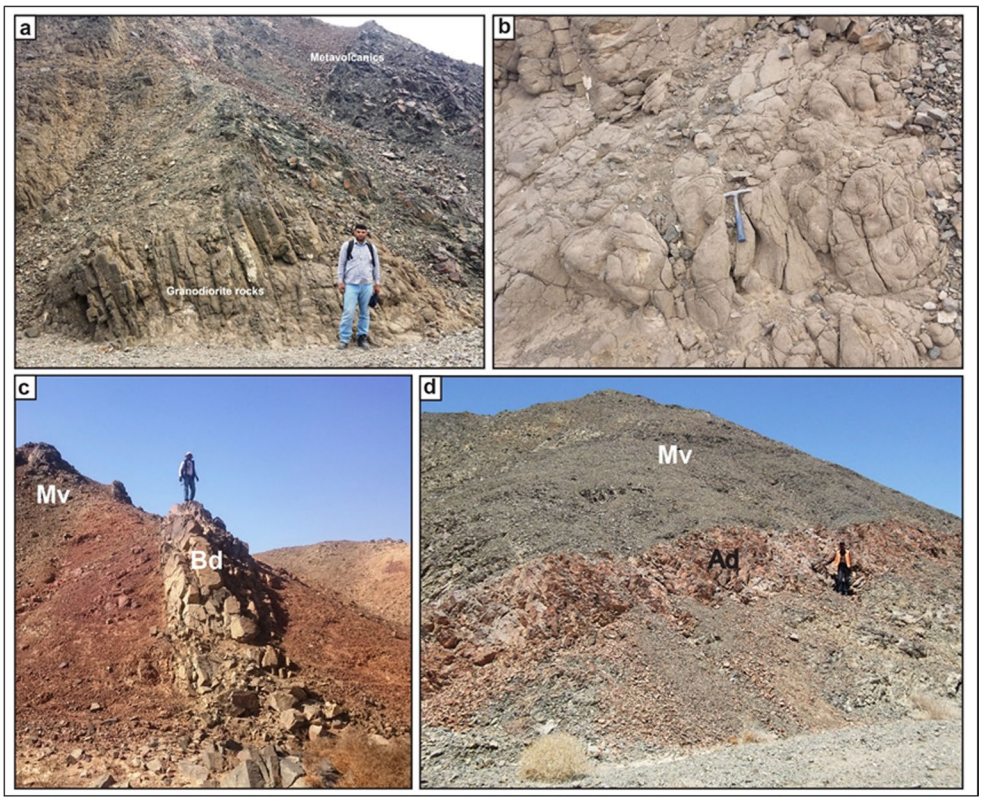


**Fig. 4** Field photographs, (**a**) Highly jointed granodiorites intruded of metavolcanics in the Wadi El Redi (Looking E), (**b**) Granodiorites showing a well-developed spheroidal weathering in Wadi El Redi (Looking NW), (**c**) Basic dike (Bd) cutting across metavolcanic (MV) rocks in the Wadi Dendekan (Looking NE), (**d**) Acidic dike (Ad) cutting across metavolcanic rocks in the Wadi Qulan el Atshan (Looking NW)

Structurally, the mineral deposits in the Atshan area are located within an E-W shear zone hosted by andesitic metavolcanics. This shear zone extends approximately 500 m in length, with a thickness ranging from 10 to 20 m. It features well-preserved penetrative foliation dipping 35° south, along with clear, graded bedding. The talc within the shear zone is commonly associated with minerals such as chlorite, tremolite, epidote, actinolite, quartz, and magnesite (calcite), as well as secondary sulfides and oxides, including malachite, azurite, hematite, and limonite gossans. Sulfide minerals present within the talc deposits include sphalerite (the dominant mineral), chalcopyrite, pyrite, and galena. The area is characterized by two primary structural trends: NE-SW and E-W. The NE-SW trend is the dominant structural feature and represents the southern extension of the Hafafit Shear Zone. Faults in this direction vary in width from 1 to 2 km [3, 27].

A detailed examination of the alteration zones around the gold-bearing quartz veins reveals that they are primarily composed of kaolinitized and highly ferruginized rocks, rich in iron oxides, and cut by numerous quartz veinlets. Some alteration zones display a significant concentration of sulfide crystals and well-developed stockwork structures. The kaolinitized zones are grayish and friable, while the ferruginized alteration zones exhibit various hues, mainly attributed to different forms of iron oxides and hydroxides (hematite and limonite).

Chemical analysis (Table 1) shows these alteration zones are enriched in gold, making them targets for extraction. The quartz veins cut through various rock units, varying in width from centimeters to meters, and extending 10 to 50 m in length (Fig. 3d). These veins typically follow NE-SW, E-W, and N-S trends. The collected samples are

**Table 1** Types, coordinates, and results of analyses of gold and associated elements of bedrock samples by Atomic Absorption (AA) analyses in the prospecting area with ppm unit

| S. No. | X | Y | Au ppm | Ag ppm | Cu ppm | Pb ppm | Zn ppm | Notes |
|---|---|---|---|---|---|---|---|---|
| S-8 | 725400 | 2684863 | 0.6 | 1.5 | 6.1 | - | - | |
| S-9 | 725410 | 2684900 | 0.3 | 0.6 | 44.3 | - | - | |
| S-2 | 725600 | 2684840 | 0.42 | 3.1 | 21.42 | 400 | 2066 | Alter. Zone |
| S-100 | 725850 | 2684840 | 0.6 | 1.1 | 17.3 | 18 | 119.5 | |
| S-200 | 725600 | 2685100 | 0.6 | 0.6 | 3 | 33.7 | 206.3 | |
| S-50 | 725380 | 2684820 | 2.82 | 1.52 | 8080 | 114.43 | 2160 | Atshan mine (Alter. Zone) |
| S-160 | 725360 | 2684800 | 7.8 | 0.8 | 13624 | 12040 | 951 | |
| Detection limits | | | 0.03 | 0.06 | 0.05 | 0.1 | 0.005 | |

selected from fresh surfaces of the main faults and quartz veins, then shipped to the laboratory for preparation for chemical analysis. The gold content and association elements were determined by Atomic Absorption (AA) analyses hosted in the Central Laboratories Sector of Egyptian Mineral Resources Authority (EMRA), Egypt. The metallic content in the selected samples is shown in Table 1. In addition to gold, there are several metallic components found, such as Silver, copper, lead, and zinc.

## 3 Methodology

To achieve the study's objectives, an integrated methodology was employed, combining geological investigations, geochemical analysis, and detailed ground geophysical surveys. The workflow was designed to characterize the mineral potential, particularly for gold and associated sulfides, within the shear and alteration zones of the metavolcanic rocks in the Atshan area. The specific methods and procedures are detailed in the following subsections.

### 3.1 Geophysical Data Acquisition

#### 3.1.1 Ground Magnetic Survey

Magnetic measurements were conducted along eleven profiles, covering a detailed area with 550 stations, using an Envi-mag proton magnetometer (Scintrex, Canada) with a sensitivity of 1.0 nT. Two instruments were employed: one served as a base station, while the other was used for field measurements along the profiles (Fig. 5). The profiles were spaced 50 m apart, and the distance between stations within each profile was 10 m. The corrected magnetic data were gridded with a 5-meter cell size using MagMap and contoured with [28]. The level of measurements above magnetized sources affects the anomalies detected by any magnetic survey, so the larger anomalies and deeper ones will be detected by an aeromagnetic survey. The advantage of the Ground magnetic survey is its ability to detect near-surface anomalies.

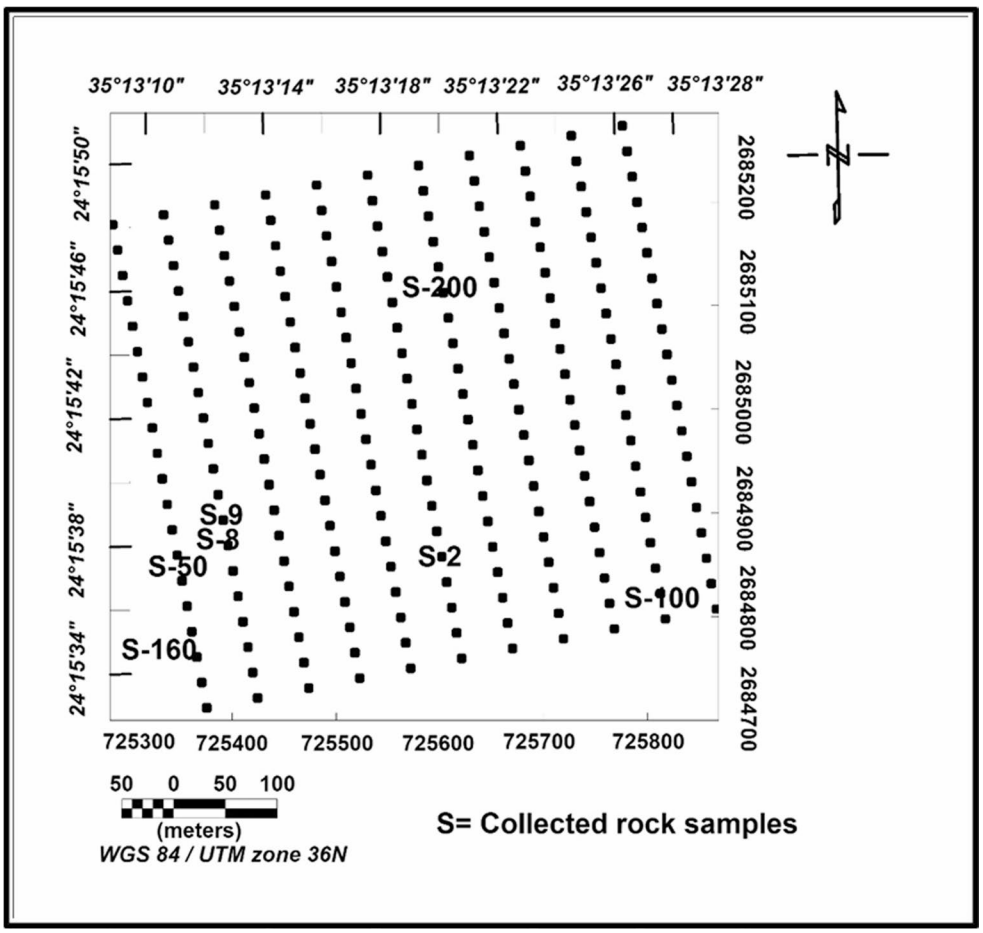


**Fig. 5** Geophysical measurement stations in addition to the geochemical samples location

#### 3.1.2 Geo-Electrical Survey

The geo-electrical survey was performed along the same profile grid. A Syscal R2 system (IRIS Company, France) was used to collect both Direct Current (DC) resistivity and Induced Polarization (IP) data simultaneously. A gradient array electrode configuration with a 5-meter electrode spacing was employed. Each of the 11 profiles contained 20 measurement stations at a 25-meter interval.

### 3.2 Data Processing

#### 3.2.1 Magnetic Data Processing

The Total Magnetic Intensity (TMI) map (Fig. 6) reveals various magnetic anomalies across different locations and trends. The eastern part exhibits moderate to high magnetic intensities, with amplitudes ranging from 41,185 to 41,440 nT, influenced by NE-trending faults. Large positive anomalies are also observed in the south-eastern, southwestern, and central areas, with amplitudes exceeding 41,440 nT. and extending in an NE direction. These anomalies are associated with metavolcanic rocks, which are highly altered (Fig. 2), and chemical rock samples (Table 1) indicate mineralization of gold and related minerals. Field investigations show that the area is dissected by structural lineaments with NE-SW, NNW-SSE, and E-W shear zone trends. Alteration zones in metavolcanic rocks, characterized by high magnetic values, are primarily located in the central, south-eastern, and southwestern regions.

#### 3.2.2 Geomagnetic Lineaments

Magnetic data can be helpful as a powerful tool for detecting lineaments, where it can detect horizontal boundaries between rock units, depending on the magnetization of each rock type. As stated by many authors, the method was described theoretically by [29, 30], who provided a foundational methodology for extracting magnetic lineaments from aeromagnetic data, emphasizing visual interpretation and manual mapping techniques. The process includes detecting parallel and elongated magnetic contours, such as linear ridges or shear zones, the alignments of magnetic highs/lows, or abrupt changes in gradient, which can detect fault zones, and mathematical filters can enhance the boundaries between rock units, like the first vertical derivative and the

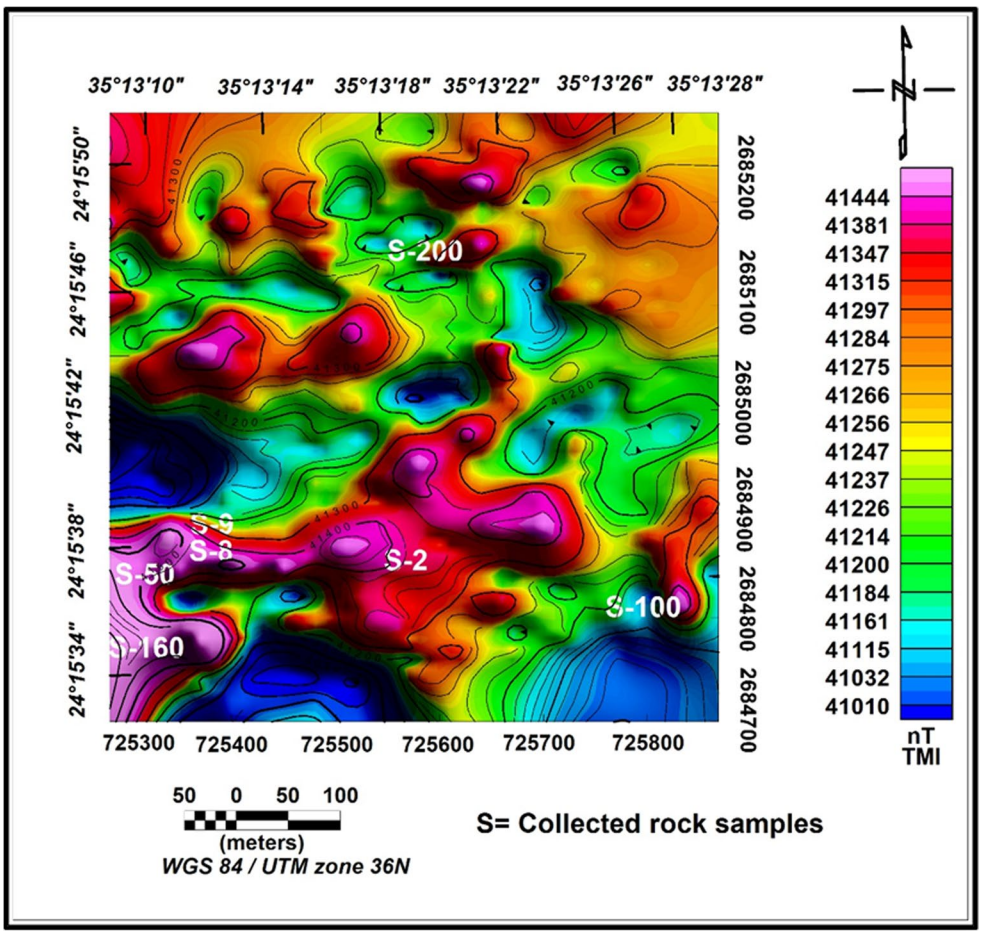


**Fig. 6** The Total magnetic intensity (TMI) map

total horizontal derivative. The method was applied by many authors in mineral exploration and groundwater [31, 32].

### 3.2.3 First Vertical Derivative (FVD) Map

The First Vertical Derivative (FVD) map is commonly employed to identify geological boundaries and edges [3, 33]. Vertical derivative maps, particularly the first or second, highlight the gradients along the boundaries of shallow causative bodies, making them effective in locating magnetic sources and emphasizing shallow depth structures [26]. Upon reviewing the first vertical derivative map (Fig. 7), it is evident that the area is influenced by NE-SW and E-W trending structural lineaments.

### 3.2.4 Horizontal Derivative (HDR)

The first-order horizontal derivatives were calculated to minimize noise in the data [34]. The horizontal gradient method (Fig. 8) quantifies the rate of change in magnetic susceptibility along the x and y axes, generating a resultant grid. The gradients are positive, making it easier to map the derivative. This method highlights linear and continuous contacts, as it solely relies on horizontal derivatives. Overall, the map emphasizes the edges and boundaries of the body, with high anomalies shown in red, indicating the locations of contacts and boundaries, and revealing structural lineaments trending NE-SW, E-W, and NW-SE.

### 3.2.5 Radially Averaged Power Spectrum

The spectral analysis technique is used to determine the depths of the basement complex, subsurface geological structures, and volcanic intrusions. This method, identified by [35, 36], relies on the Fourier Transform of potential field data, such as gravity and magnetic data, to analyze the wavelengths in both X and Y directions. The average depth and regional-residual separation are determined from the slope of a line fitted to the linear segment of the curve using the equation:

$$h = -S \cdot 4\pi \tag{1}$$

Where h is the depth, and S is =slope of the log (energy) spectrum.

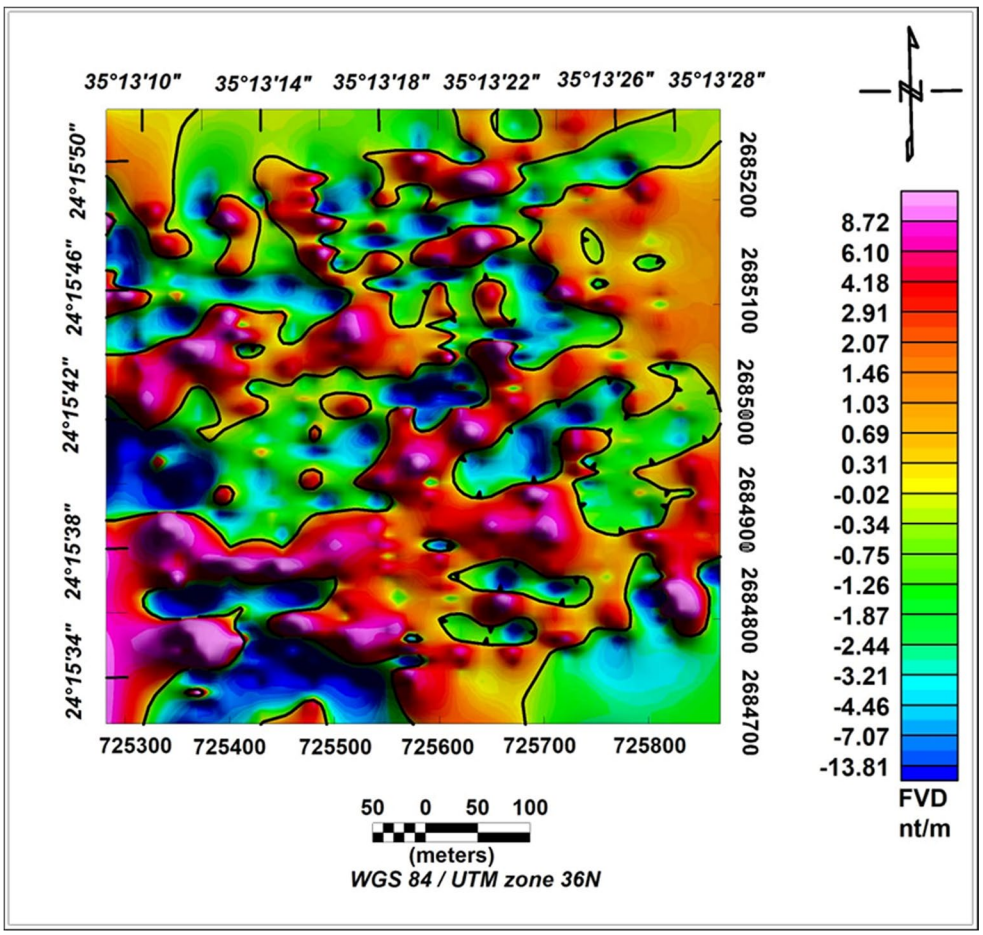


**Fig. 7** The first vertical derivative (FVD) magnetic map, including the zero-contour line, enhances the boundaries between different rock units

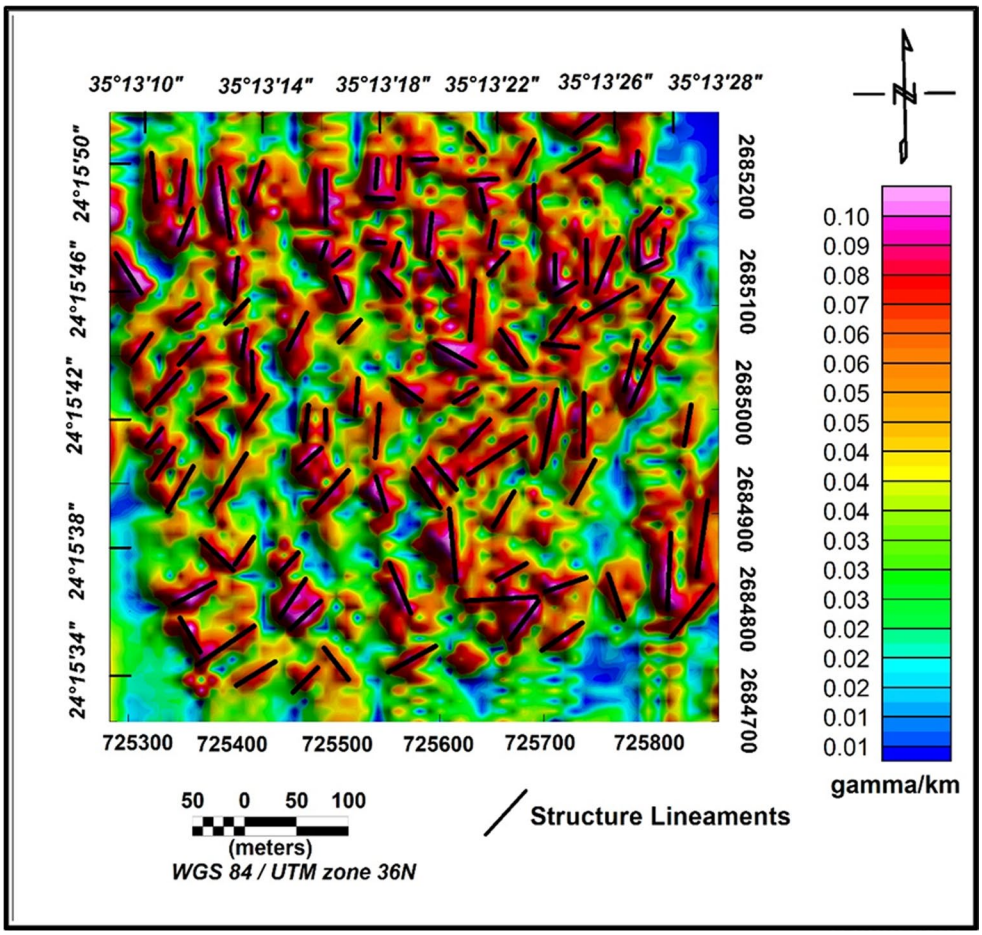


**Fig. 8** Horizontal derivative (HDR)map

In this study, the azimuth-averaged power spectrum method [35] was used to estimate the top of the source bodies causing the magnetic anomalies. The logarithmic plot of the power spectrum against the inverse wavenumber (Fig. 9) revealed three segments. The first segment corresponds to deep regional sources, with a depth of about 30–35 m; the second segment reflects intermediate sources at a depth of 15–25 m; and the third segment, representing shallow or residual sources, is located at depths of 10–15 m.

#### 3.2.6 Source Parameter Imaging (SPI)

The source parameters can be estimated from gridded magnetic data using Geosoft [28]. The Source Parameter Imaging (SPI) method (Fig. 10) [27] determines the source edge by calculating the reciprocal of the local wave number.

$$Depth\,(x=0) = 1/K_{max} \tag{2}$$

where $K_{max}$ Represents the peak value of the local wavenumber at the source edge.

### 3.3 Geo-Electrical Data Processing

A geo-electrical survey was conducted along the same geomagnetic profiles (see Fig. 5) and contains 11 profiles having trending N330ºW on a grid pattern, each profile divided into 20 stations. The distance between the two profiles is 50 m, and the interval spacing between the two stations is 25 m.

#### 3.3.1 Electrical Resistivity

Electrical exploration is a key geophysical technique used to identify subsurface structures and mineral deposits. It has been applied to mineral exploration [37–39], subsurface pipe mapping [40], site remediation [41], and bedrock channel mapping [42].

The resistivity value (ρ) is calculated using:

$$\rho_a = G\,\frac{\triangle V}{I} \tag{3}$$

Where: G is the geometric factor of the electrode arrangement that equals:

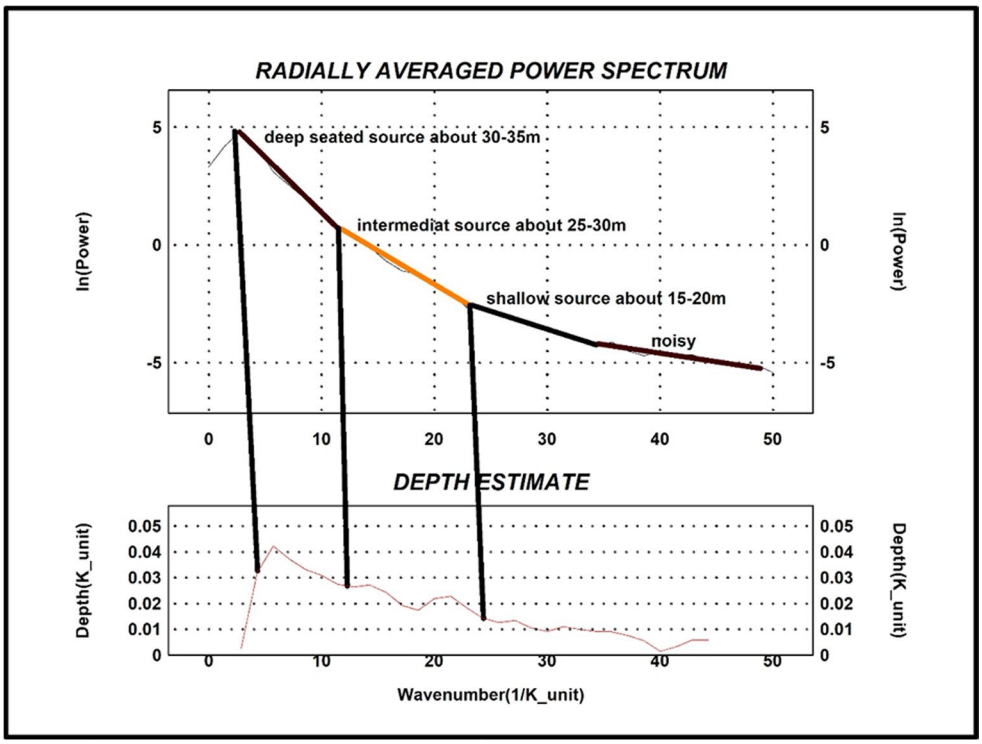


**Fig. 9** Radial average Power spectrum as an analytic method for depth estimate

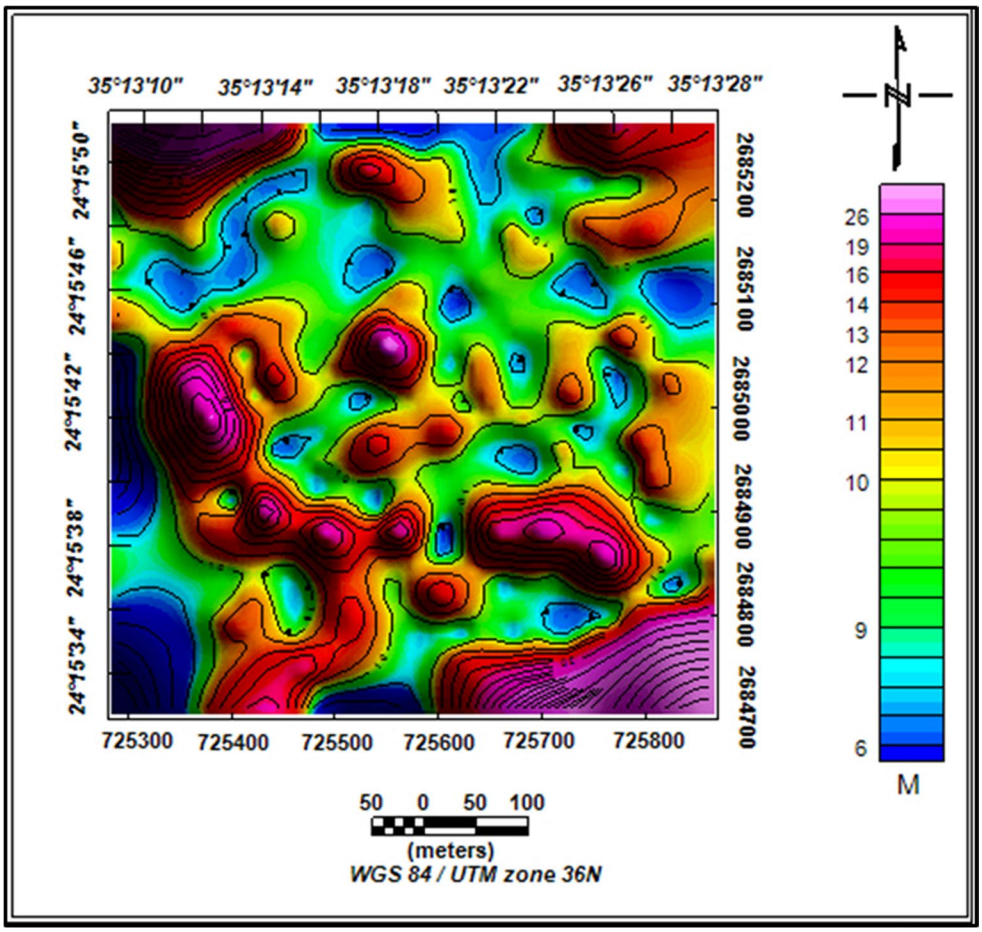


**Fig. 10** Source Parameter Imaging (SPI) with depths to both shallow and deep magnetized sources

$$G = 2\pi / \left( \frac{1}{r1} - \frac{1}{r2} - \frac{1}{r3} + \frac{1}{r4} \right) \quad (4)$$

Where: r1, r2, r3, and r4 are the distances between current and potential electrodes. The resulting value of resistivity (ρ) is often referred to as the "apparent" resistivity ( $\rho_a$), especially in inhomogeneous or anisotropic environments, as explained by [43]. The resistivity measurements are collected using a gradient array for both resistivity and IP using Syscal R2 of IRIS Company-France with electrode spacing of 5 m.

The apparent resistivity map (Fig. 11) shows zones of low to medium resistivity, particularly in the western and southeastern areas, which correspond to mineralized regions containing gold and associated minerals. These anomalies align with the NNE-SSW and E-W directions. The map also reveals a middle zone with high-frequency, small-width anomalies located in the central and northern parts of the area. These low-resistivity zones are likely related to shear zones, alteration zones, or the presence of sulfide minerals, which are controlled by hydrothermal fluid paths and structural features.

### 3.3.2 Induced Polarization (IP)

Induced polarization (IP) is a geophysical phenomenon where earth materials exhibit a delayed voltage response to electrical stimulation. It has become an effective method in the exploration of disseminated sulfide ores [44] and is increasingly used in geophysical surveys. This relatively recent technique is primarily applied in the exploration of base metals [45].

The gradient chargeability map (Fig. 12) reveals a range of small amplitudes from 1 to 52 mSec, which dominate most of the area. High chargeability values are observed in the western and eastern edges of the map, while the central region shows lower to moderate values. This distribution of chargeability anomalies suggests the presence of shallow to near-surface causative bodies.

### 3.3.3 Resistivity/IP -Wenner- Schlumberger Profiles (P1 and P2)

It is a hybrid between the Wenner and Schlumberger arrays, rising out of relatively recent work with electrical imaging surveys. Two-dimensional electrical imaging tomography surveys

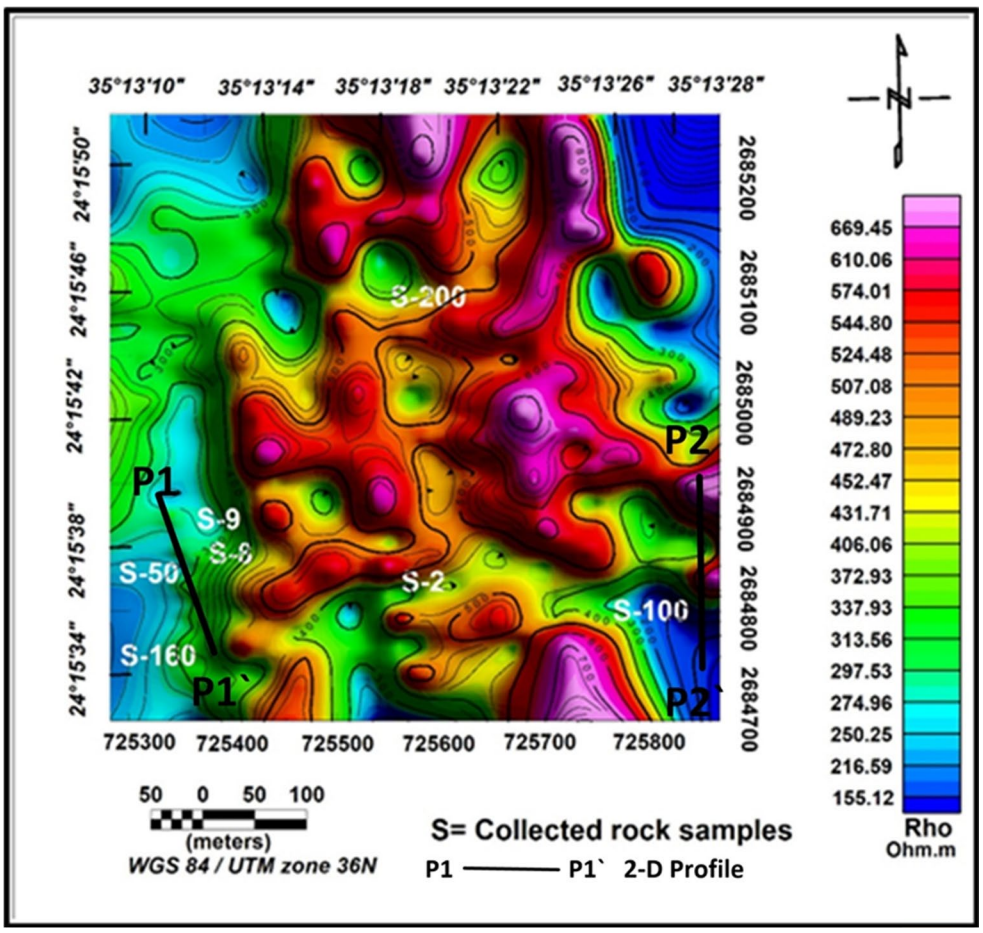


**Fig. 11** The Resistivity map of the area illustrates the horizontal distribution of resistivity across the region

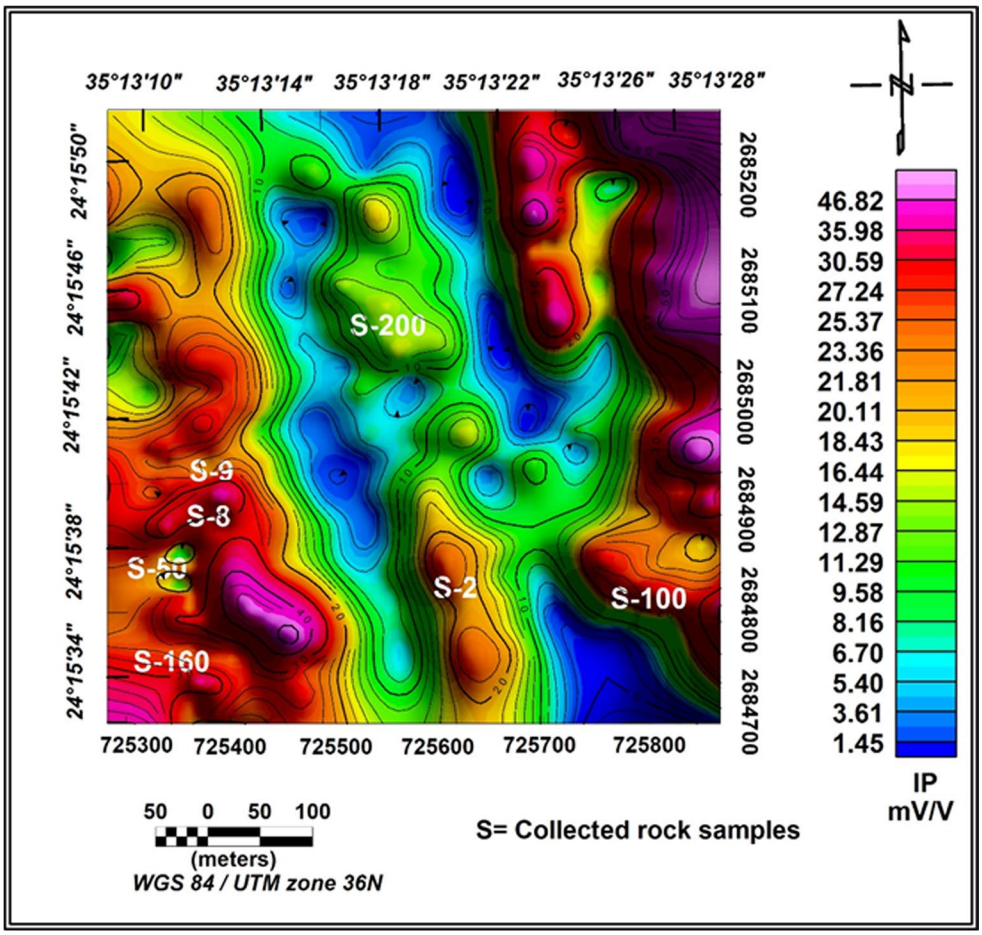


**Fig. 12** The gradient IP (Induced Polarization) map of the area illustrates the horizontal distribution of chargeability across the region

are usually carried out using many electrodes, 25 or more, connected to a multi-core cable. In this research, the location of 2-D Wenner-Schlumberger array profiles (Fig. 11) with 32 electrodes connected to two multi-core cables 80 m long was applied to recording measurements. The inversion was then carried out to detect the true resistivity. The inversion technique of the least squares was used to allow the modeling of relatively sharp changes in resistivity/IP because the inversion algorithm aims to minimize the absolute value of data misfit.

## 4 Geoelectric Section along Profile P1-P1′

The profile P1-P1` of length is about 155 m and its depth is about 31 m (Fig. 13), which is located in the southwestern part, and shows three zones of high chargeability and low resistivity. The first one is found at a distance of about 90 m from the start of the profile within a depth range of 20–25 m, while the second causative body appears at a distance of about 100 m. at a depth of about 5–6 m, and the third ore body appears at a distance of about 120 m from the section with a depth of about 10–15 m.

## 5 Geoelectric Section along Profile P2-P2′)

The profile P2-P2` of length is about 155 m, and its depth is about 30 m (Fig. 14), which lies in the south-eastern part, and shows three places of low resistivity and relatively high chargeability. The first one is at a distance of about 85 m with a depth of 24 to 28 m. In comparison, the second ore body appears at a distance of about 93 m within a depth range of 8–10 m, and the third high chargeability-low resistivity zone is detected at a distance of about 135 m from the section within a depth of about 6–8 m.

## 6 Results and Discussion

The integration of geological, geochemical, and geophysical data in this study has successfully delineated the key characteristics and controls of gold mineralization in the Atshan area. The results are presented and discussed below, synthesizing the findings from each method to build a coherent exploration model.

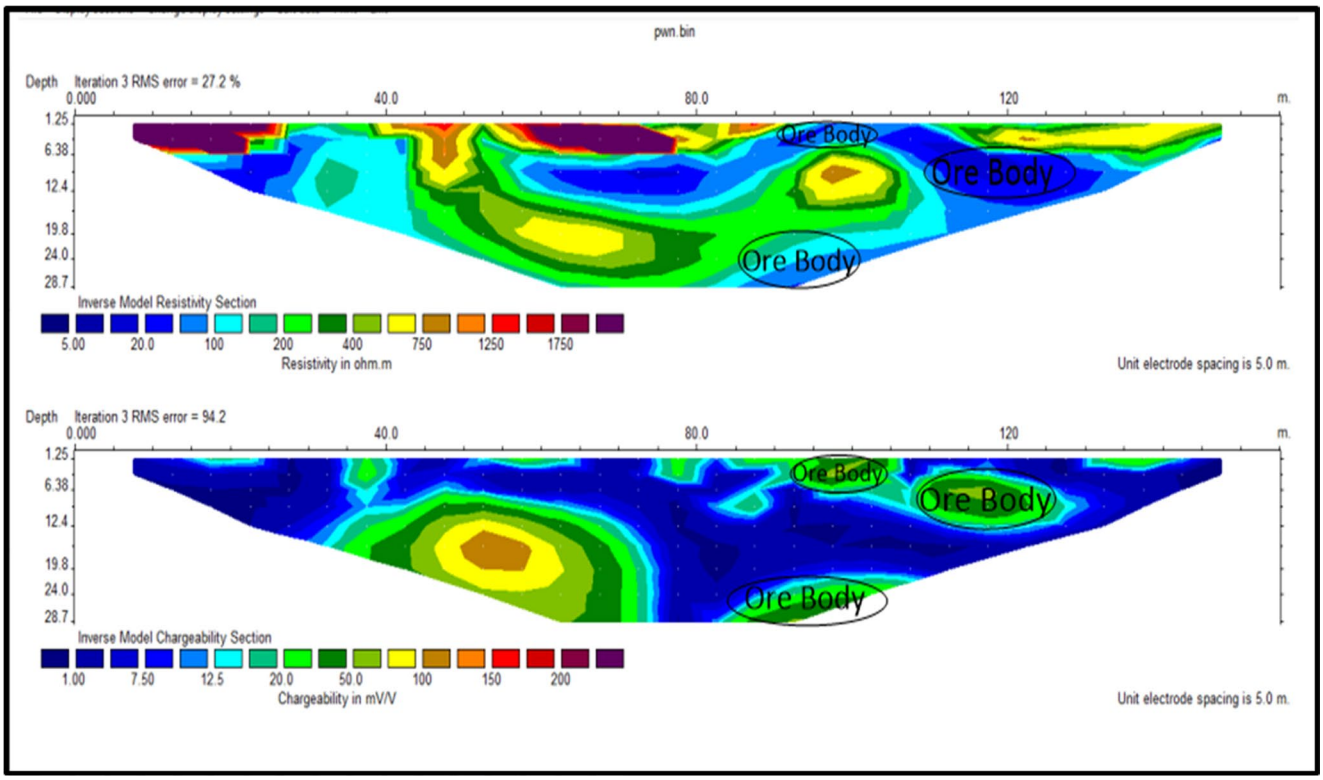


**Fig. 13** Wenner- Schlumberger array along profile (P1-P1`), showing some high chargeability low resistivity bodies that may be related to mineralization

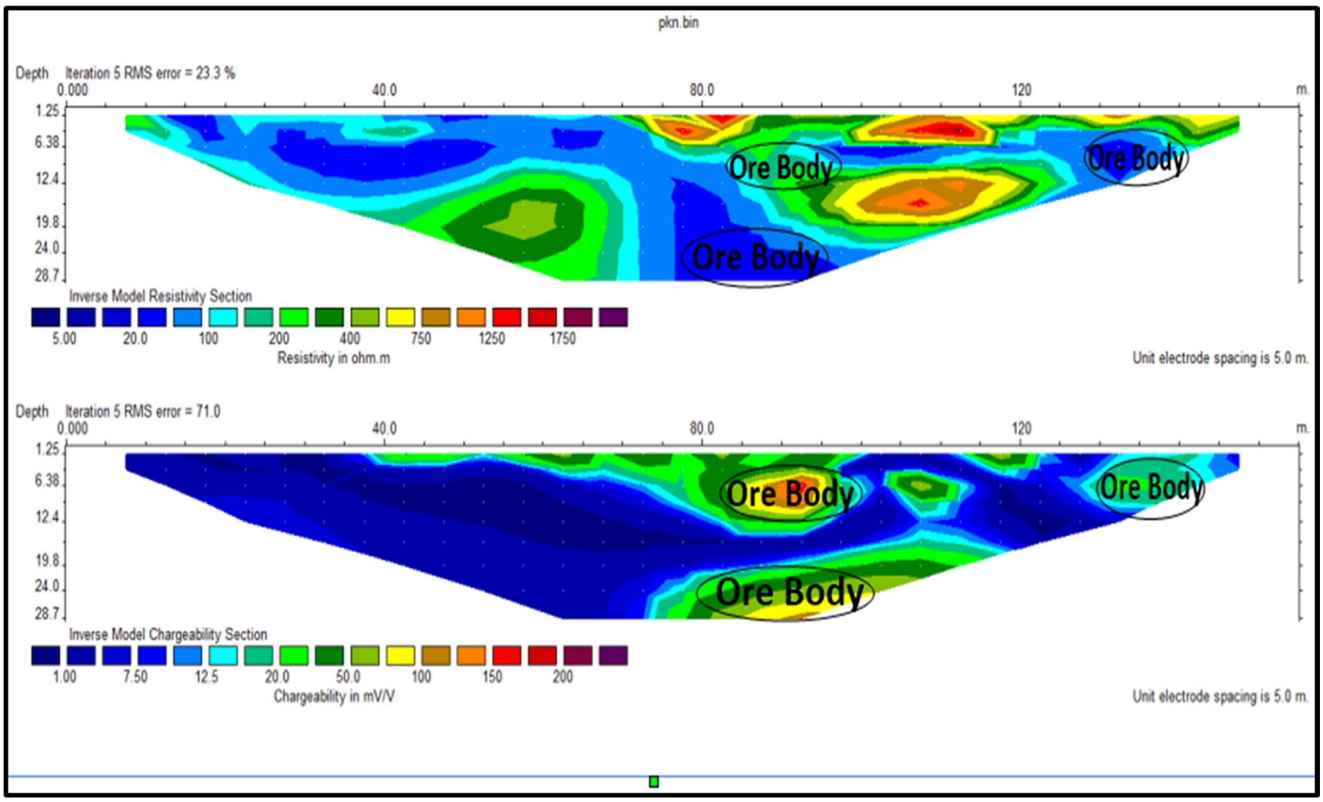


**Fig. 14** Wenner- Schlumberger array along profile (P2-P2`), showing some high chargeability low resistivity bodies that may be related to mineralization

### 6.1 Integration of Geophysical Anomalies and Geochemical Verification

The correlation between geophysical anomalies and geochemical data forms the core of this study's findings. As illustrated in Fig. 15, zones of high magnetic intensity, low electrical resistivity, and high chargeability show a strong spatial correlation. These geophysical signatures are interpreted as indicators of mineralized zones.

- **High Magnetic Anomalies**: The Total Magnetic Intensity (TMI) map (Fig. 6) revealed significant anomalies, with values exceeding 41,440 nT in the southwestern, south-eastern, and central parts of the study area. These high-amplitude anomalies are associated with the metavolcanic rock unit, which is known to be sheared and altered (Fig. 2). The magnetic highs likely result from the presence of magnetite and/or pyrrhotite, which can be associated with hydrothermal alteration systems. Depth estimates from the Radially Averaged

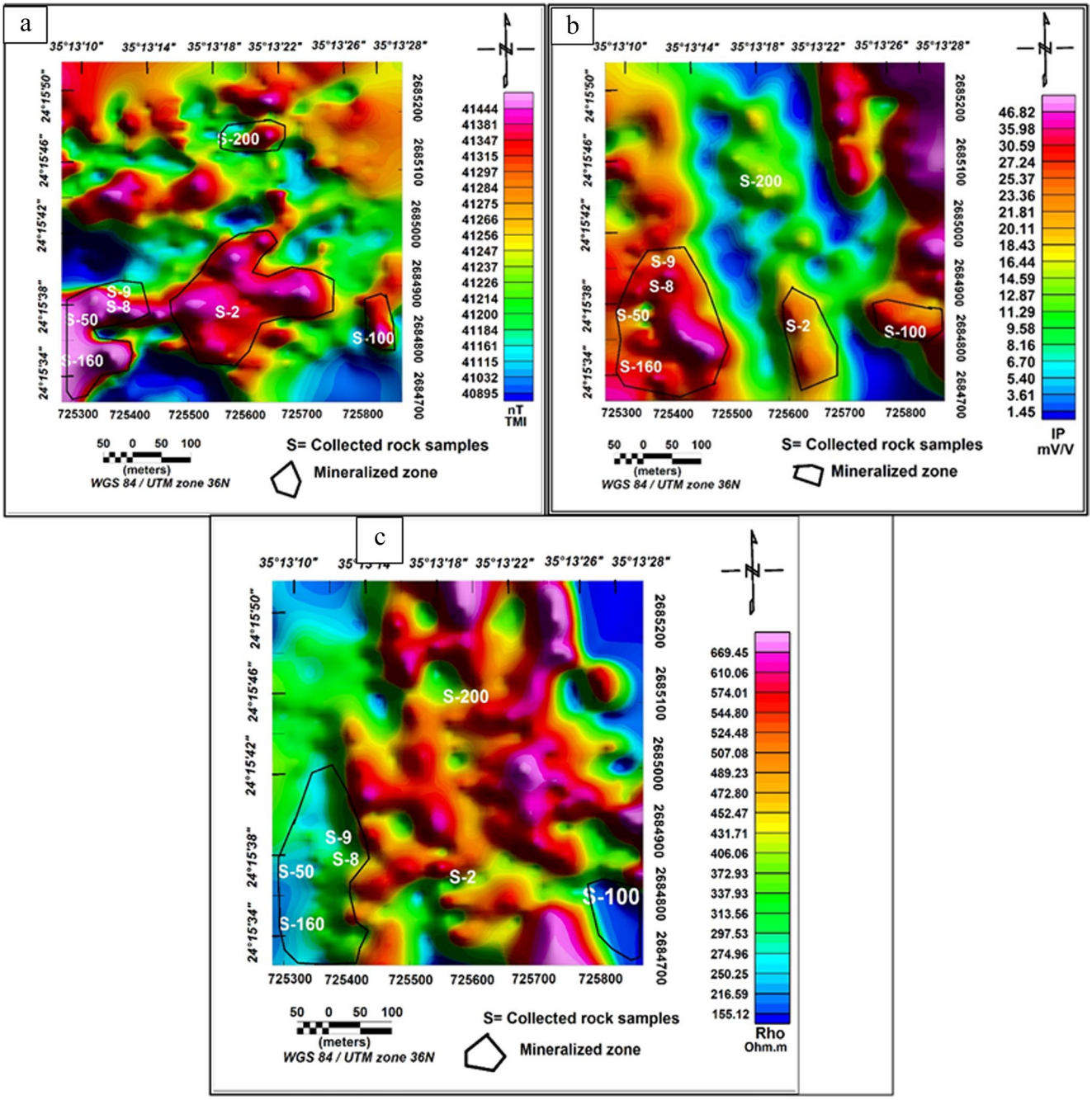


**Fig. 15** Various geophysical anomalies with rock samples: (**a**) total magnetic intensity. (**b**) induced polarization (**c**) electrical resistivity maps

Power Spectrum (Fig. 9) and Source Parameter Imaging (SPI, Fig. 10) indicate that the causative bodies for these anomalies are relatively shallow, ranging from 5 to 40 m, making them viable targets for near-surface exploration.

- **Low Resistivity and High Chargeability Zones**: The resistivity map (Fig. 11) identified prominent zones of low resistivity (generally < 200 ohm·m) in the western and south-eastern sectors. Concurrently, the Induced Polarization (IP) map (Fig. 12) showed high chargeability anomalies (up to 52 mSec) along the western and eastern edges of the survey area. The co-location of low resistivity and high chargeability is a classic geophysical signature of sulfide mineralization. Low resistivity is typically caused by the presence of electronically conductive minerals like graphite or interconnected sulfide networks (e.g., pyrite, chalcopyrite), while high chargeability is a direct indicator of dissaminated sulfide minerals.

The validity of these geophysical anomalies as indicators of mineralization is strongly supported by the geochemical data (Table 1). Rock samples collected from these anomalous zones, particularly samples S-50 and S-160 from the Atshan mine alteration zone, returned highly elevated values not only for gold (up to 7.8 ppm) but also for associated pathfinder elements like copper (up to 13,624 ppm), lead (up to 12,040 ppm), and zinc (up to 2,160 ppm). This clear correlation confirms that the identified geophysical anomalies are not artifacts but represent genuine zones of sulfide mineralization enriched in gold and base metals.

### 6.2 Delineation of Mineralized Bodies in 2D Section

The 2D electrical resistivity tomography (ERT) and IP inversions along profiles P1 and P2 (Figs. 13 and 14) provide a vertical perspective that corroborates the map-based interpretations. These sections reveal discrete, subsurface bodies characterized by low resistivity and high chargeability.

- Along profile **P1** (Fig. 13), three such bodies were identified at depths ranging from 5 to 6 m to 20–25 m.
- Profile **P2** (Fig. 14) also shows three causative bodies at depths between 6 and 8 m and 24–28 m.

The identification of multiple, sub-vertical bodies at various depths suggests a stockwork or vein-type mineralization pattern, which is consistent with the observed surface geology of quartz veinlets and stockworks within alteration zones (Fig. 3e). The variable depth of these bodies indicates that mineralization is not confined to a single horizon but is distributed within the shear zone, likely controlled by structural conduits.

### 6.3 Structural Control on Mineralization

A key finding of this study is the pronounced structural control on the mineralization. The integration of surface geological mapping with derivative magnetic maps (FVD and HDR) reveals a consistent structural framework.

The Horizontal Derivative (HDR) map (Fig. 8) and First Vertical Derivative (FVD) map (Fig. 7) were crucial in enhancing structural lineaments. The integrated structural map (Fig. 16) demonstrates that the primary structural trends in the Atshan area are NE-SW, E-W, and NW-SE. These trends show excellent compatibility between subsurface (geophysical) and surface (geological) data.

The NE-SW trend is the most dominant and is interpreted as the southern extension of the regional Hafafit Shear Zone. The E-W trend corresponds directly to the mapped shear zone hosting the talc deposits and gold-bearing quartz veins. These structural features acted as primary conduits for hydrothermal fluids, facilitating water-rock interaction, alteration, and the subsequent deposition of sulfide and gold mineralization. The convergence or intersection of these trends likely created zones of enhanced permeability and dilation, forming high-grade shoots and stockworks, as evidenced by the high geochemical values in samples from these areas.

### 6.4 Synthesis: A Conceptual Exploration Model

Based on the integrated results, a conceptual exploration model for gold mineralization in the Atshan area is proposed:

1. **Host Environment**: Mineralization is primarily hosted within intermediate metavolcanic rocks (metaandesites) that have undergone intense shearing and hydrothermal alteration.
2. **Structural Trap**: The primary control is an E-W trending shear zone, with secondary control from NE-SW and NW-SE fault systems. These structures channelled mineralizing fluids.
3. **Geophysical Expression**: The mineralized zones are characterized by a coincident geophysical signature of:

- High magnetic intensity (likely from magnetite alteration).
- Low electrical resistivity (from conductive sulfide minerals and clay alteration).
- High chargeability (from disseminated sulfide mineralization).

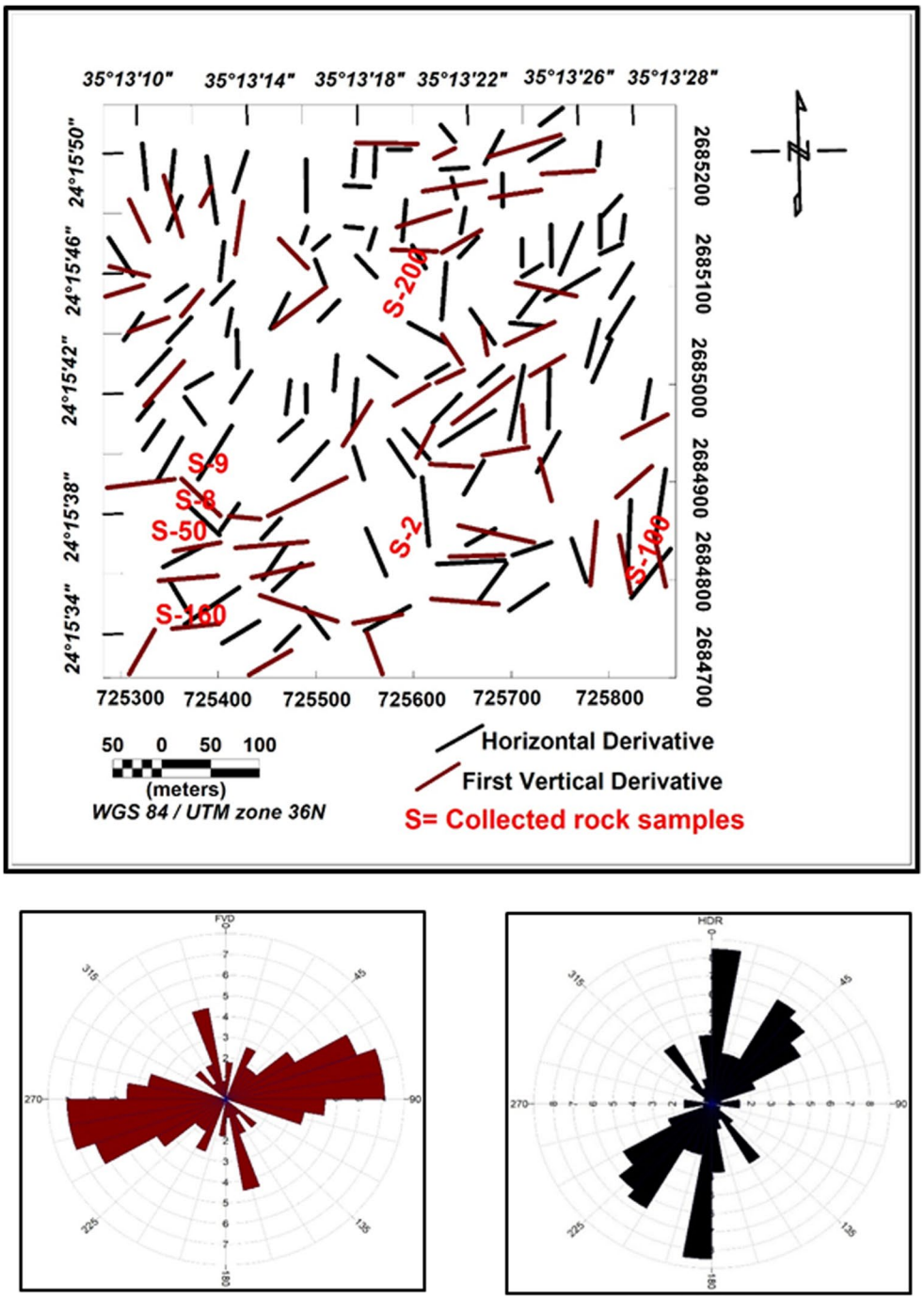


**Fig. 16** Structural trends as determined by Horizontal derivative (HDR) (black rose diagram) and first vertical derivative (FVD) (brown rose diagram), and rock samples

4. **Geochemical Signature**: These zones are enriched in Au, Ag, Cu, Pb, and Zn, with gold often encapsulated within sulfide minerals.

The most promising targets for future exploration are, therefore, areas where these geophysical, geochemical, and structural criteria overlap, particularly in the western, central, and south-eastern parts of the study area.

## 7 Conclusion

This integrated geological, geochemical, and geophysical study successfully delineates the controls and potential of gold mineralization in the Atshan area. The mineralization is conclusively structurally controlled, hosted within sheared and hydrothermally altered intermediate metavolcanic rocks (metaandesites) along a major E-W trending

shear zone, with secondary influences from NE-SW and NW-SE fault systems.

The research demonstrates a robust correlation between geophysical anomalies and geochemical verification. Zones of high magnetic intensity (>41,440 nT.), low electrical resistivity (<200 ohm·m), and high chargeability (up to 52 mSec) show a strong spatial coincidence with known surface mineralization and returned highly elevated gold values of up to 7.8 ppm, along with significant concentrations of pathfinder elements like copper, lead, and zinc. Depth estimation techniques indicate that these mineralized bodies are shallow, occurring within 5 to 40 m of the surface, making them highly viable targets for near-surface exploration.

The 2D geo-electrical sections further confirm the presence of discrete, sub-vertical mineralized bodies exhibiting the characteristic low-resistivity and high-chargeability signature, supporting a stockwork or vein-type mineralization model. The synthesis of these datasets provides a validated, data-driven exploration model for the Atshan area, highlighting the western, central, and south-eastern sectors as the most prospective zones for gold and associated sulfide minerals.

## 8 Recommendations

Based on the findings of this study, the following actions are recommended to advance exploration and evaluate the economic potential of the Atshan area:

1. **Targeted Drilling Campaign**: Immediate follow-up with a systematic drilling program is essential. Priority should be given to the high-priority targets identified in the western, central, and south-eastern parts of the study area, where geophysical anomalies, geochemical assays, and structural controls converge. Drilling will verify the subsurface extent, continuity, and grade of the mineralized bodies identified in the 2D sections.
2. **Expanded Geochemical Survey**: Conduct a more extensive and detailed geochemical survey, including soil and rock chip sampling on a denser grid. This will help to define the geochemical holes better, identify new anomalies, and vector towards the highest-grade zones of mineralization.
3. **High-Resolution Geophysical Surveys**: Implement further detailed ground geophysical surveys over the identified targets. Using closer station spacing for magnetic, resistivity, and IP methods will provide higher-resolution data to guide drill hole placement precisely.
4. **Structural Geology Analysis**: A dedicated structural geology study, including detailed mapping and kinematic analysis, is recommended to fully understand the geometry and evolution of the shear and fault systems. This will help predict the location of high-grade shoots within the larger mineralized zones.
5. **Mineralogical and Metallurgical Studies**: Perform detailed mineralogical studies (e.g., using SEM and XRD) on drill core samples to determine the mineral hosts for gold (e.g., free within quartz or encapsulated in sulfides) and the textural relationships. Preliminary metallurgical tests should also be conducted to assess gold recovery rates, which are critical for economic evaluation.

By implementing these recommendations, the promising mineralization in the Atshan area can be systematically evaluated, moving from a conceptual model to a defined resource with clear economic potential. The integrated approach demonstrated in this study can also serve as an effective blueprint for exploration in similar geological terrains within the Arabian-Nubian Shield.

**Funding** Open access funding provided by The Science, Technology & Innovation Funding Authority (STDF) in cooperation with The Egyptian Knowledge Bank (EKB).

**Data Availability** The datasets used and/or analyzed during the current study are available from the corresponding author upon reasonable request.

## Declarations

**Competing Interest** The authors have no competing financial or non-financial interests that are relevant to the content of this article. The authors declare that they have no competing interests. The authors review the spelling and grammar through some colleagues of native English.



## References

1. Sultan SA, Mansour SA, Santos FM, Helaly AS (2009) Geophysical exploration for gold and associated minerals at Wadi El Beida Area, South-eastern Desert, Egypt, journal of geophysics and engineering, 6:345-356 . https://doi.org/10.1088/1742-2132/6/4/002
2. Zoheir BA, Emam A (2012) Application of ASTER data to lithological mapping and ore mineral exploration: case study from the Fawakhir area, Eastern desert of Egypt. Arab J Geosci 5(5):1055–1068. https://doi.org/10.1007/s12517-011-0280-6

3. Horo D, Pal SK, Singh S (2021) Mapping of Gold Mineralization in Ichadih, North Singhbhum Mobile Belt, India using electrical resistivity tomography and self-potential methods. Mining, Metallurgy & Exploration 38:397–411. https://doi.org/10.1007/s42461-020-00340-4
4. El Lasheen SR, Mohamed WH, Mahmoud H, Elyaseer, Mohamed A, Rashwan, Mokhles K, Azer (2023) Geochemical and remote sensing integrated with satellite gravity data of Darhib and Atshan Talc deposits, South Eastern Desert, Egypt. Sci Rep 13:91–108. https://doi.org/10.1038/s41598-023-31398-x
5. Abdel-Karim A-AM (2022) Genesis of sulfide mineralization, Atshan and Darhib Areas, South Eastern desert of egypt: evidence of fluid pathway effects along shear zones. Arab J Sci Eng 47:641–665
6. Othman AAA, Fathy M, Mebed M, El Rahmany M, Hammam AF (2014) Application of integrated geophysical methods to delineating probable area of metallic mineralization at Wadi El Homer at the South of Marsa Alam City, South Eastern Desert, Egypt. New York Sci J 7(4):P71–81
7. Schandl ES, Gorton MP, Sharara NA (2002) The origin of major Talc deposits in the Eastern desert of egypt: relict fragments of a metamorphosed carbonate horizon? J Afr Earth Sci 34:259–273
8. Araffa SAS, Rabeh TTT, Mousa SEDAW et al (2020) Integrated geophysical investigation for mapping of manganese-iron deposits at Wadi al Sahu area, Sinai, Egypt—a case study. Arab J Geosci 13:823. https://doi.org/10.1007/s12517-020-05869-8
9. Mousa SAW, Abdel Nabi SH, Araffa SAS et al (2020) Geophysical exploration of titanomagnetite ore deposits by geomagnetic and geoelectric methods. SN Appl. Sci. 2:444. https://doi.org/10.1007/s42452-020-2206-5
10. Horo D, Pal SK, Singh S, Biswas A (2023) New insights into the gold mineralization in the Babaikundi–Birgaon axis, North Singhbhum mobile Belt, Eastern Indian shield using magnetic, very low-frequency electromagnetic (VLF-EM), and self-potential data. Minerals 13:1289. https://doi.org/10.3390/min13101289
11. Chen W, Xuanqing Z, Naihua H, Yonghong M (1996) Compiling the map of shallow-buried paleochannels on the North China Plain. Geomorphology 18:47–52
12. Ramadan TM, Sultan AS (2004) Integration of remote sensing, geological and geophysical data for the identification of massive sulphide zones at Wadi Allaqi area. J. Earth Sci. 18:165–74. https://doi.org/10.1109/IGARSS.2003.1294520
13. Spector A (1975) : Application of aeromagnetic data for porphyry copper exploration in areas of volcanic cover, the 45th Ann. Inter. Meeting of the Society of Exploration Geophysics, October 15, Denver, Colorado, U.S
14. Amer RM, Kusky TM, El-Mezayan A (2011) Remote sensing detection of gold related alteration zones in Um-Rus area, central Eastern desert of Egypt. J Adv Space Res 49:121–134
15. Akaad MK, Noweir AM (1980) Geology and lithostratigraphy of the Arabian Desert Orogenic Belt of Egypt between latitudes 25º 35` and 26º 30` N. I.A.G. Bull., Jeddah 2:127–136
16. El Ramly MF, Akaad MK (1960) : The Basement Complex in the Central Eastern Desert of Egypt between Latitudes 24º 30` and 25º 40` N. Geol. Surv. Egypt, Paper No.8, 35p.https://books.google.com.eg/books/about/The_Basement_Complex_in_the_Central_East.html?id=j9VGAAAAYAAJ&redir_esc=y
17. El-Gaby S, List FK, Tehrani R (1990) The basement complex of the Eastern Desert and Sinai. In: R., Said, (ed.), The Geology of Egypt, BalkemaRotterdam-Bookfield, Holland, 175–184. https://doi.org/10.1201/9780203736678
18. Waheed H, Mohamed MH, Elyaseer, Mohamed Elsadek M, Sabra (2023) Structural lineament analysis of the Bir El–Qash area, central Eastern Desert, Egypt, using integrated remote sensing and aeromagnetic data. Sci Rep 13(1):21569. https://doi.org/10.1038/s41598-023-48660-x
19. Hassan AM, Hashad AH (1990) : Precambrian of Egypt. In: The Geology of Egypt (Edited by Said, R.) Balkema, Rotterdam, Brookfield. 201–248.
20. Masoud MS (1994) Geological map of Sheikh shadli-Hamata district, South Eastern desert, Egypt. Internal report 36/94, Geol. Surv. Egypt, Cairo
21. Mostafa Mo (1996) Geological map of Tarafawi-Abu Ghusun area, South Eastern desert, Egypt. Internal report 2/96, Geol. Surv. Egypt, Cairo
22. Hussein AAA, Ali MM, El-Ramly MF (1982) A proposed new classification of the granites of Egypt. J Volcanol Geoth Res 14:187–198
23. Kroner A, Greiling R, Reisch mann T, Hussein IM, Stern RJ, Kruger J, Zimmer M (1987) Pan-African crustal evolution in the Nubian segment of Northeast Africa. Ann Geophy Union Spec Publ 17. https://doi.org/10.1029/GD017p0235
24. Ramadan TM, Sultan SA (2003) Integration of geological, remote sensing and geophysical data for the identification of massive sulphide zones at Wadi Allaqi Area, South Eastern Desert, Egypt, IGARSS 2003. 2003 IEEE International Geoscience and Remote Sensing Symposium. Proceedings (IEEE Cat. No.03CH37477), Toulouse, France, 2589–2592. https://doi.org/10.1109/IGARSS.2003.1294520
25. Henderson RG, Zietz I (1949) The computation of second vertical derivatives of geomagnetic fields. Geophysics 14:477–561
26. Dobrin MB, Savit CH (1990) : Introduction to geophysical prospecting, 4th edition, McGraw-Hill Book Co., 867 P
27. Thurston JB, Smith RS (1997) Automatic conversion of magnetic data to Depth, Dip, and susceptibility contrast using the SPI (TM). Method: Geophys 62:807–813. https://doi.org/10.1190/1.1444190
28. Geosoft (2015) Geosoft Oasis Montaj, Ver. 8.4 software for Earth science. Geo-soft Inc., Toronto, Canada. https://my.geosoft.com/
29. Gay S (1972) Fundamental characteristics of aeromagnetic lineaments, their geological significance, and their significance to geology. The new basement Tectonics; American stereo map company. Salt Lake, UT, USA
30. Solomon T, Owolabi K, Madi AM, Kalumba C, Baiyegunhi A geomagnetic analysis for lineament detection and lithologic characterization impacting groundwater prospecting; a case study of Buffalo catchment, Eastern Cape, South Africa,Groundwater for sustainable Development,12,2021,100531,ISSN 2352–2801X, https://doi.org/10.1016/j.gsd.2020.100531
31. Al Deep M, Ibrahim AS, Saleh A (2024) Geophysical assessment of structurally controlled mineral resources at Wadi El-Nakheel, Eastern desert. Egypt Resour 13(6):83. https://doi.org/10.3390/resources13060083
32. Araffa SAS, Abdulattif A, Al Deep M, Khozym A, Salama H, Gaweish WR, Ebrahim S (2025) Integrated geophysical and hydrochemical assessment of groundwater aquifers for agricultural development: a case study in the area South Alamein-Wadi El Natrun road. Egypt all Earth 37(1):1–17. https://doi.org/10.1080/27669645.2025.2463735
33. Clarke KG (1969) Optimum second-derivative and downward continuation filters. Geophysics 34:424–437. https://doi.org/10.1190/1.1440020
34. Phillips JD (1998) Processing and interpretation of aeromagnetic data for the Santa Cruz Basin-Patagonia mountains area, South –central Arizona, U.S. Geophysical survey open –file report. 2002–2098. https://doi.org/10.3133/ofr0298
35. Spector A, Grant FS (1970) Statistical models for interpreting aeromagnetic data. Geophysics 35:293–302. https://doi.org/10.1190/1.1440092
36. Bhattacharya BK (1965) Two-dimensional harmonic analysis as a tool for magnetic interpretation. Geophysics 30:829–857

37. Botros N.S. (2004) A new classification of the gold deposits of Egypt. Ore Geol Rev 25:1–37
38. Ramage JM, Gardner TW, Sasowsky ID (1998) Early Pleistocene Glacial Lake Lesley, West Branch Susquehanna River Valley, Central Pennsylvania. Geomorphology 22:19–37
39. Gilson EW, Nimeck G, Bauman PD, Kellett R (2000) : Ground Water Exploration In Prairie Environments, In Powers, M.H., Ibrahim, A., Cramer, L., Eds., Proceedings of the Symposium On The Application of Geophysics To Engineering And Environmental Problems: Wheat Ridge, Colorado, Environmental And Engineering Geophysical Society, 955–959
40. Noel M, Xu B (1991) Archaeological investigations by electrical resistivity tomography: a preliminary study. J Geophys 107:95–102. https://doi.org/10.1111/j.1365-246X.1991.tb01159.x
41. Bentley LR, Gharibi M (2004) Two- and three-dimensional electrical resistivity imaging at a heterogeneous remediation site. Geophysics 69:674–680
42. Vickery AC, Hobbs BAThe Effect of Subsurface Pipes on Apparent Resistivity Measurements:Geophysical Bulletin, 57, 10–48., Vincent RK (2002) (1997): Fundamental of geological and environmental remote sensing. Prentice-Hall. Inc. USA. 366p. https://doi.org/10.1046/j.1365-2478.2002.00295.x
43. Zohdy AAR (1974) : Electrical Methods in Application of Surface Geophysics to Groundwater Investigations, Books 2, Chapter D1, US Department of the interior, 5–66. https://doi.org/10.3133/twri02D1
44. Ramzey M, Abd El-Rahman Y, Said A (2021) Weathering products at the historic Qulaan gold prospect, Eastern Desert, Egypt: implication on the mobility and distribution of arsenic, gold and silver. J Afr Earth Sci 182:104276
45. Stern RJ, Johnson PR, Kröner A, Yibas B (2004) Neoproterozoic ophiolites of the Arabian-Nubian shield. In: Kusky TM (ed) Precambrian ophiolites and related Rocks, developments in precambrian geology, vol 13. Elsevier, Amsterdam, pp 95–128